THERMAL CHARACTERISTICS ANALYSIS OF MEDIUM FREQUENCY TRANSFORMER UNDER MULTIPLE WORKING CONDITIONS

Pei HUANG[a,b*], Tong SHEN[a,b], Zhenxing LIU[a,b], Renjun DIAN[a,b], Wanlun XU[a,b], and Dan WANG[c,d]

[a]School of Information Science and Engineering, Wuhan University of Science and Technology, Wuhan 430081, China

[b]Engineering Research Center for Metallurgical Automation and Measurement Technology of Ministry of Education, Wuhan University of Science and Technology, Wuhan 430081, China

[c]State Key Laboratory of Advanced Electromagnetic Engineering and Technology, Huazhong University of Science and Technology, Wuhan 430074, China

[d]School of Electrical and Electronic Engineering, Huazhong University of Science and Technology, Wuhan 430074, China

[*] Corresponding author; E-mail: huangpei0722@163.com

Medium frequency transformer (MFT) plays an important role in high power AC-DC transformation in power grid, due to its high power density and high loss density, it brings difficulty to heat dissipation. Thermal reliability is crucial for transformer design, different from the previous work, the thermal characteristics of MFT under different working conditions are concerned and analyzed in this paper. The temperature field model of MFT is established, and the temperature field characteristics of MFT at rated load, no load, overload, fluctuating overload and short circuit conditions are simulated and analyzed, the results show that with the increase of load coefficient, the winding temperature increases obviously, the allowable load coefficient of MFT can be determined by calculating the transformer temperature at different load coefficients, which lays a foundation for thermal reliability and safe operation of MFT.

Key words: *medium frequency transformer, thermal analysis, temperature field, transformer safety*

1. Introduction

With the increase of DC loads such as renewable energy [1], electric vehicles [2] and energy storage [3] in power grid, a large amount of AC-DC power conversion [4] is indispensable. Among them, medium frequency transformer (MFT) [5-10] is the key component, which plays the role of potential isolation and voltage conversion. By increasing the working frequency, the volume and weight of MFT are reduced, however, the loss density increases and the heat dissipation area decreases, resulting in heat dissipation difficulties. Temperature rise is a very important performance index of transformer, if it exceeds the limit, the transformer insulation life expectancy is affected and

in an extreme case the transformer can result in permanent damage [11]. Therefore, thermal characteristics analysis and heat dissipation design are the crucial issues in MFT design.

Thermal analysis and cooling design of transformers have been studied in previous work [12-16]. The comprehensive thermal analysis of the structure parts and winding area of oil-immersed auto-transformer are performed in [12], the use of an arrangement of wall shunts is proposed to reduce the transformer temperature rises. The thermal management of the magnetic core and winding components for compact transformers operating at high frequency is studied in [13], new configurations are designed to reduce thermal stress. In order to analyze the temperature distribution more comprehensively, an improved thermal network method for MFT is proposed in [14]. The temperature distribution of a layered winding natural cooling type distribution transformer is researched in [15], and the impact of several parameters on temperature distribution is analyzed. A 3-D frequency-dependent thermal model based on lumped parameters network for planar transformers is proposed in [16], which provides a powerful and fast design tool to evaluate the temperature distribution.

Some achievements have been made in temperature field analysis and heat dissipation design of MFT [5,7,9,17,18], however, most of the heat dissipation design is carried out under rated working condition. The maximum temperatures of MFT at no-load and rated load were simulated in [5], and a heat dissipation scheme combining fin array heat exchanger and forced air cooling was adopted, in order to ensure high power density of MFT, the dimension of fin array heat exchanger was optimized. The hot spot temperature of MFT is solved by a detailed steady-state thermal network model in [7], and the temperatures of MFT at no-load and rated-load steady-state are measured to verify the thermal characteristic. A novel cooling structure which utilizes two layers 3-D printed bobbins is proposed in [9], the 3-D printed structure can provide airflow channels for core and windings. A dc bias current capacity is used as a design constraint in the optimization of MFT in [17], and temperature distribution of MFT at no load and full load are measured to verify the design method. Two thermal management methods are applied in [18], heat sinks are placed on the core surface to increase the heat dissipation area, and a thermally conductive material is placed between the windings and core to conduct heat to the heat sinks. It can be seen that the above research on MFT mainly carries out temperature field analysis based on rated working conditions.

For the power grid, the load demands are now more volatile than ever before, because of new generation and consumption technologies such as renewable energy and electric vehicles, and the load of transformer can be daily fluctuant, which submits the transformer to the risk of overload [19]. However, the existing studies on MFT [17,18] mainly carry out thermal analysis for rated working conditions, ignoring severe working conditions such as overload and fluctuating overload, and it is difficult to ensure the safety under special working conditions.

Different from previous work, this paper makes a comprehensive analysis of temperature field characteristics under various working conditions, the influences of special working conditions including overload and fluctuating overload on temperature field are fully considered to ensure the reliability of MFT. The temperature field model of a 35 kW MFT is established, and the temperature field characteristics of MFT at rated load, no load, overload, fluctuating overload and short circuit conditions are researched and analyzed, the temperature field distribution, average temperature and highest temperature are studied, and the influences of different load conditions on transformer

temperature field are discussed, which provide a basis for guiding MFT safe operation, and also have important reference value for fault diagnosis, aging research and cooling scheme design of MFT.

2. Working condition analysis of MFT

MFT may work in overload condition because of the dynamic change of load in power grid, and the load coefficient is used to evaluate the overload state of transformer. The load coefficient K is defined as follow:

$$K = \frac{P_2}{P} \tag{1}$$

where P_2 is actual output power, and P is rated output power.

It is generally recommended that the maximum load coefficient K of dry type transformer should not exceed 1.5, therefore, the working conditions at load coefficients of 0.8-1.6 are studied in this paper, including 0.8, 0.9, 1.0, 1.1, 1.2, 1.3, 1.4, 1.5, and 1.6. Besides, the no-load, variable load and short circuit conditions are also researched. The working voltage of MFT decreases a little under overload, while the working current of MFT increases with the increasing of load coefficient. According to the principle of loss [8], core loss is related to excitation voltage, and winding loss is related to winding current, therefore, the increase of load coefficient leads to the change of core loss and winding loss.

In order to calculate the winding loss under different load coefficient, the winding currents under different load coefficient should be calculated and analyzed, then the winding loss at fundamental and harmonic frequencies can be obtained.

3. Temperature field modeling of MFT

3.1. Calculation method of temperature field

The temperature field analysis of the transformer obeys the heat conduction eq. (2) [20]. In the process of fluid temperature coupling, the fluid governing equations, namely, the mass conservation equation, the momentum conservation equation and the energy conservation equation, should be observed.

$$\rho c \frac{\partial T}{\partial t} = k\left(\frac{\partial^2 T}{\partial x^2} + \frac{\partial^2 T}{\partial y^2} + \frac{\partial^2 T}{\partial z^2}\right) + Q \tag{2}$$

Where T is the surface temperature of each part of the transformer, k is the thermal conductivity coefficient, c is the specific heat capacity, ρ is the material density, and Q is heat source intensity.

Air is regarded as a non compressible fluid, which follows the law of conservation of mass in the flow process, as shown in eq. (3) [21].

$$\frac{\partial \rho}{\partial \mathrm{t}} + \rho\left(\frac{\partial u}{\partial x} + \frac{\partial v}{\partial y} + \frac{\partial w}{\partial z}\right) = 0 \tag{3}$$

Where ρ is the air density, u, v, w are the components of the fluid velocity field vector on the x, y, z coordinate axes respectively.

The momentum conservation equation is shown in eqs. (4), (5), and (6) [22].

$$\frac{\partial(\rho u)}{\partial t}+div(\rho uU)=\frac{\partial \rho}{\partial x}+\frac{\partial \tau_{xx}}{\partial x}+\frac{\partial \tau_{yx}}{\partial y}+\frac{\partial \tau_{zx}}{\partial z}+F_x \tag{4}$$

$$\frac{\partial(\rho v)}{\partial t}+div(\rho vU)=\frac{\partial \rho}{\partial y}+\frac{\partial \tau_{xy}}{\partial x}+\frac{\partial \tau_{yy}}{\partial y}+\frac{\partial \tau_{zy}}{\partial z}+F_y \tag{5}$$

$$\frac{\partial(\rho w)}{\partial t}+div(\rho wU)=\frac{\partial \rho}{\partial z}+\frac{\partial \tau_{xz}}{\partial x}+\frac{\partial \tau_{yz}}{\partial y}+\frac{\partial \tau_{zz}}{\partial z}+F_z \tag{6}$$

Where F_x, F_y, F_z is the volume force density, U is the velocity vector, and τ_{xx}, τ_{yx} and τ_{zx} are the components of the viscous stress τ effecting the surface of infinitesimal control volume produced by molecule viscous effect.

The energy inside the transformer is transmitted in the form of heat energy, which follows the law of energy conservation, as shown in eq. (7) [23].

$$\rho c\cdot\left(\frac{\partial T}{\partial t}+\nabla(uT)\right)+\nabla\cdot q=Q \tag{7}$$

Where u is the fluid velocity vector, c is the specific heat capacity, T is the fluid temperature, q is the heat flux, and Q is heat source intensity.

3.2. Specifications and parameters of MFT

A case study on MFT in electric power transformer application is carried out in this paper, its rated capacity is 35 kW, operating frequency is 1 kHz, maximum primary voltage is 1500V, and maximum secondary voltage is 385V. The RMS values of fundamental wave of primary and secondary winding current under different load coefficients are shown in tab. 1, and the core loss and winding loss of this MFT at different load coefficients are provided in tab. 2.

Table 1. The RMS values of fundamental wave of primary and secondary winding current under different load coefficients.

Load coefficient	0.8	0.9	1.0	1.1	1.2	1.3	1.4	1.5	1.6
Primary winding current/A	13.83	16.33	18.18	21.54	24.18	28.36	30.32	35.26	40.27
Secondary winding current/A	52.30	62.05	69.29	82.40	92.71	109.00	116.70	136.00	155.50

Table 2. Core loss and winding loss at different load coefficients.

Load coefficient	0.8	0.9	1.0	1.1	1.2	1.3	1.4	1.5	1.6
Core loss/W	235.4	229.6	225.5	219.0	214.1	205.3	198.9	191.1	183.4
Winding loss/W	144.0	199.2	245.0	338.2	420.0	562.7	676.9	812.0	1044.3

3.3. Temperature field modeling of 35 kW MFT

This core-type MFT is modeled in multi-physical field software COMSOL as shown in fig. 1. The length, width and height of core are 190mm, 100mm, and 270mm respectively. The length, width

and height of HV winding are 118mm, 170mm, and 146mm respectively, and the length, width and height of LV winding are 88mm, 140mm, and 146mm respectively. The transformer core, formed by stacking multiple layers of silicon steel sheets, is simplified into a single entity. The LV winding is simplified as an inner-layer square winding, and the HV winding is simplified as an outer-layer square winding. The fluid heat transfer module is added and configured. The heat source in this model includes core loss and winding loss. The core loss and winding loss are calculated separately. There are three ways to set the heat source in the simulation model, and one of them is chosen— the heat rate. The calculated core loss value is used as the heat rate of heat source of the core, and the calculated winding loss value is used as the heat rate of heat source of the winding in the simulation model. The air is natural convection. The model is established based on two assumptions: (a) The ambient temperature is 20 degrees Celsius; (b) The transformer is not damaged due to excessive temperature. The materials of core and winding are silicon steel and copper respectively, the heat transfer coefficient of silicon steel is 42.5W·(m·K)$^{-1}$, and that of copper is 398W·(m·K)$^{-1}$.

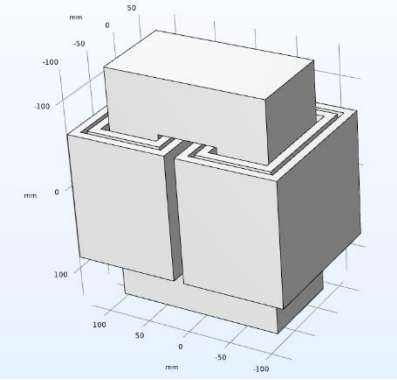

Figure 1. The temperature field model of 35 kW MFT.

4. Temperature field calculation under different working conditions

4.1. Temperature field calculation at rated load

When MFT works at rated load, the core loss is 225.5W, and the winding loss is 245W, the steady-state temperature distribution of MFT is shown in fig. 2. The highest temperature occurs in the core, and the lowest temperature occurs in the HV winding.

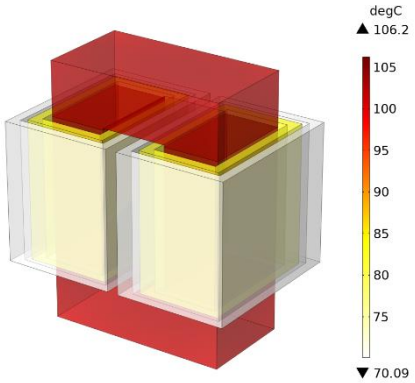

Figure 2. The steady-state temperature distribution of MFT at rated load.

The steady-state temperature distribution of core is shown in fig. 3(a), the core column is surrounded by winding and it is difficult to dissipate heat, therefore, its temperature is slightly higher

than that of the yoke. The steady-state temperature distribution of HV winding is shown in fig. 3(b), the highest temperature occurs in two sides of the left and right windings located inside the core window, while the other three surfaces in contact with the air have better heat dissipation.

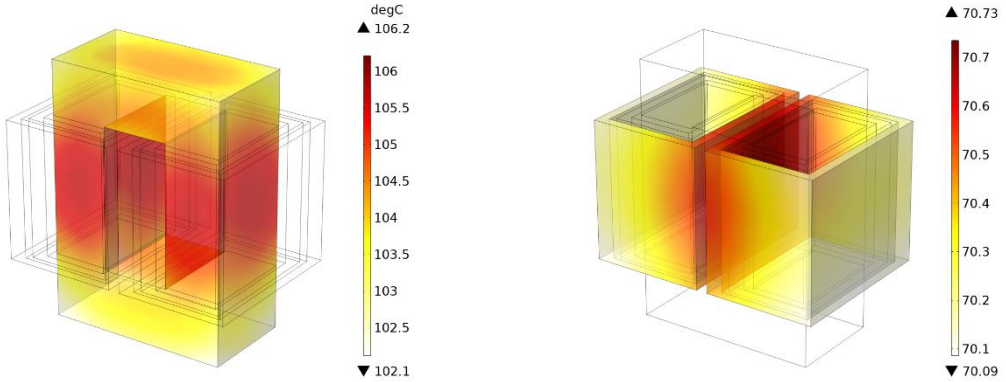

(a) **(b)**

Figure 3. The steady-state temperature distribution of core and HV winding at rated load. (a)Core. (b)HV winding.

The average temperature of core, LV winding, and HV winding varies with time as shown in fig. 4, the temperature rises gradually with time for core and windings. It takes about 3 hours for the HV windings to reach steady state, while it takes about 6 hours for the core to reach steady state.

The average and highest temperature of core, LV winding, and HV winding are provided in tab. 3. There is a very small difference between the average and highest temperature, indicating that the temperature distribution is relatively uniform. The LV winding is sandwiched between the core and HV winding, the heat dissipation area is small, while the HV winding is surrounded by air outside, thus, the temperature of LV winding is higher than that of HV winding.

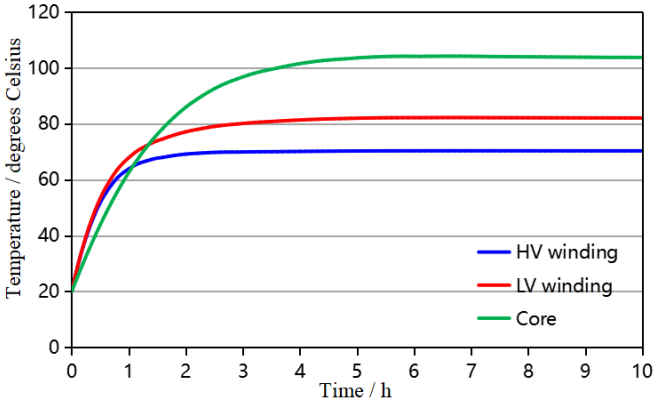

Figure 4. The average temperature of core, LV winding, HV winding varies with time at rated load.

Table 3. The temperature field calculation results at rated load.

	HV winding	LV winding	Core
Average temperature/℃	70.39	82.36	104.85
Highest temperature/℃	70.74	82.43	106.21

4.2. Temperature field calculation at no load

When MFT works at no load, the excitation voltage is rated and the core loss is 225.5W, while the primary and secondary winding currents are 0 A, thus the winding loss is 0 W. The simulation results of the average temperature and highest temperature of the core, LV winding, and HV winding under no load conditions are shown in tab. 4. The highest temperature of core is 98.99 degrees Celsius, which is lower than the results at rated load in tab. 3, since the total loss of MFT decreases at no load. The average and highest temperature of windings are much lower than the results at rated load as shown in tab. 3, since there is no winding loss at no load, and the temperature rise of winding mainly comes from the heat dissipation of core.

Table 4. The temperature field calculation results at no load.

	HV winding	LV winding	Core
Average temperature/℃	25.29	40.39	98.14
Highest temperature/℃	25.33	40.43	98.99

4.3. Temperature field calculation at load coefficient of 1.2

When MFT works at load coefficient 1.2, the core loss is 214.1W, and the winding loss is 420W. The average and highest temperature values of core, LV winding, HV winding are provided in tab. 5. The winding current increases with the increase of load coefficient. The winding loss is proportional to the square of the winding current, resulting in the significant increase of winding loss and significant rise of winding temperature. From Table 2, it can be observed that the core loss decreases with the increase of the load coefficient, so the core temperature should have decreased. However, there is heat transfer between the winding and core, resulting in an increase of core temperature. In addition, due to the gap between the winding and core, the heat transfer is limited, so the core temperature does not rise much. Compared with the rated load condition, when the load coefficient increases to 1.2, the core loss reduces a little, while the winding loss is increased by 1.7 times, leading to the significant increase of winding temperature.

Table 5. The temperature field calculation results at load coefficient 1.2.

	HV winding	LV winding	Core
Average temperature/℃	95.91	106.76	107.09
Highest temperature/℃	96.49	106.85	108.80

4.4. Temperature field calculation at load coefficient 1.4

When MFT works at load coefficient 1.4, the core loss is 198.9W, and the winding loss is 676.9W. The average and highest temperature values of core, LV winding, HV winding are provided in tab. 6. Compared with the rated load condition, when the load coefficient increases to 1.4, the winding loss is increased by 2.8 times, resulting in a large increase in winding temperature.

Table 6. The temperature field calculation results at load coefficient 1.4.

	HV winding	LV winding	Core
Average temperature/℃	128.87	138.86	111.56
Highest temperature/℃	129.83	138.97	113.88

4.5. Comparison of temperature field results at different load coefficients

The average and highest temperature of LV winding and HV winding at different load coefficients are shown in fig. 5. The increase of load coefficient leads to the increase of winding current, winding loss, and winding temperature. The insulation grade of this MFT is F, and the temperature limit is 155 degrees Celsius. With the increase of the load coefficient, the temperature will reach the limit, which may damage the insulation and cause failure. Therefore, the allowable load coefficient of the transformer can be determined by calculating the transformer temperature at different load coefficients.

The average temperature values of core at different load coefficients are provided in tab. 7. The core loss reduces a little with the increase of load coefficient, however, the core temperature is affected by the winding temperature, which increases a little with the increase of winding temperature.

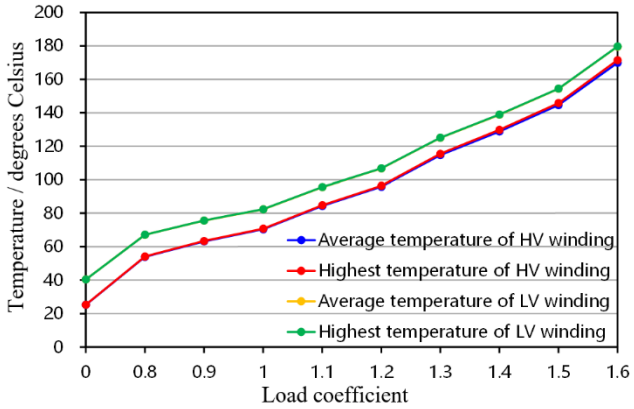

Figure 5. The average and highest temperatures of LV winding and HV winding at different load coefficients.

Table 7. The average temperature values of core at different load coefficients.

Load coefficient	0	0.8	0.9	1.0	1.1
average temperature /℃	98.14	104.63	104.64	104.85	105.89
Load coefficient	1.2	1.3	1.4	1.5	1.6
average temperature /℃	107.09	109.38	111.56	114.31	120.92

4.6. Temperature field calculation at variable load condition

MFT temperature field at variable load condition is researched, and variable load condition refers to the change of load coefficient. MFT works at rated load from 0-4.2 h, and works at load coefficient of 1.2 during 4.2~10 h, therefore, the winding loss increases from 245W to 420W at 4.2 h, and the core loss decreases from 225.5W to 214.1W at 4.2h, as shown in fig. 6.

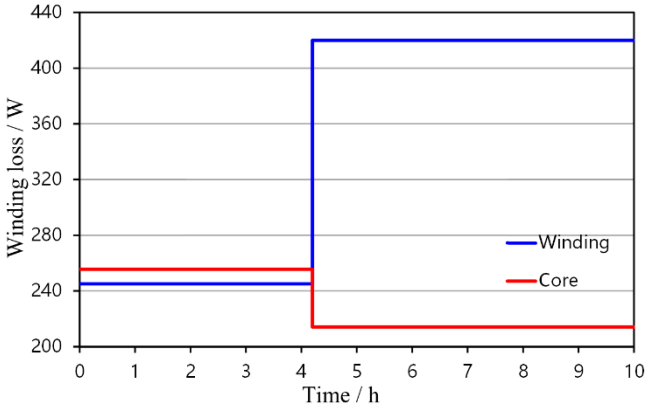

Figure 6. The winding loss and core loss varies with time at variable load condition.

The average temperature of core, LV winding, and HV winding varies with time as shown in fig. 7, the temperature of windings reached basic stability at about 3 h, and continued to increase at 4.2 h, and reached stability again at about 6 h, the average temperature of LV winding and HV winding are stable at 95.9 and 106.73 respectively. At the same time, the core temperature reached stability at about 7 h and remained stability, which was not affected by the load mutation. The change of load coefficient influences the winding current and leads to the increase of winding loss and winding temperature, while the change of load coefficient leads to a little change of the core loss, thus the change of load coefficient does not lead to significant change of core temperature.

The average and highest temperature values of core, LV winding, and HV winding are provided in tab. 8, which is basically the same as the results at load coefficient of 1.2 as shown in tab. 5, since MFT works at load coefficient of 1.2 during 4.2-10 h.

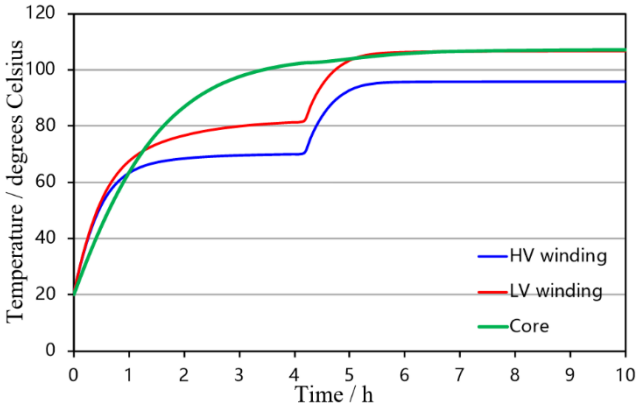

Figure 7. The average temperature of core, LV winding, HV winding varies with time at variable load condition.

Table 8. The temperature field calculation results at variable load condition.

	HV winding	LV winding	Core
Average temperature/℃	95.90	103.73	106.96
Highest temperature/℃	96.48	106.82	108.68

4.7. Temperature field calculation at short-circuit fault

When a short circuit fault occurs in the load of the DC-DC converter where the MFT is working at, the resulting short-circuit current is much higher than the normal working current of MFT, thus, the winding loss is greatly increased, resulting in a huge increase in temperature. The simulation results at

short circuit condition show that the temperature difference between the core and the windings is significant, and both are much higher than that of rated conditions. The average temperature of core, LV winding, and HV winding varies with time as shown in fig. 8. In the first half-hour, the temperatures of the windings and core rise rapidly, and after half an hour, the temperatures of the windings and core reach and maintains stability. Table 9 provides the average and highest temperature values of the core, LV winding, and HV winding. Compared with rated load conditions, when a short-circuit fault occurs on the load side, the winding loss increases by 461 times, causing a sharp rise in the winding temperature, and the core temperature also increases significantly due to the influence of the winding temperature, which is far beyond the temperature range that the transformer can withstand, which will lead to transformer damage.

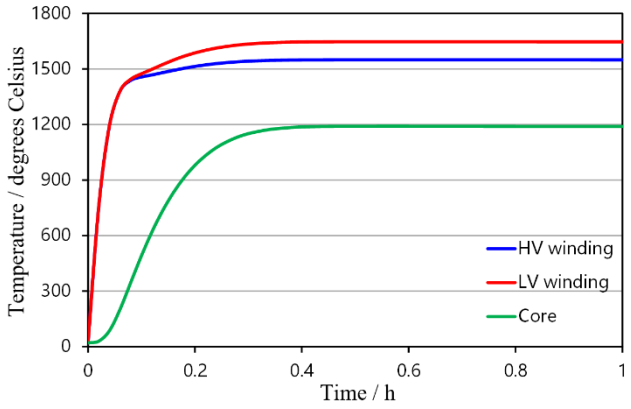

Figure. 8. The average temperature of core, LV winding, HV winding varies with time at short-circuit fault condition.

Table 9. The temperature field calculation results at short-circuit fault condition.

	HV winding	LV winding	Core
Average temperature/℃	1550.21	1648.07	1190.32
Highest temperature/℃	1781.00	1739.84	1638.95

5. Conclusion

This paper is devoted to the temperature field modeling and analysis of MFT, the temperature distribution characteristics and the influences of load coefficient variation on the temperature field of MFT are studied, the main work is as follows:

(a) The temperature field model of MFT using 3-D finite element method is established, the temperature field distribution, average temperature and highest temperature can be obtained.

(b) The temperature field distribution of MFT at rated load is simulated, and the results show that the highest temperature occurs in the core, and the lowest temperature occurs in the HV winding, the temperature of core column is slightly higher than that of the yoke, and the highest temperature of windings is located in the core window.

(c) The temperature field distributions of MFT at different load coefficients are simulated and compared, the results show that with the increase of load coefficient, the winding temperature increase obviously, while the increase of core temperature is small, besides, the allowable load coefficient of MFT can be determined by calculating the transformer temperature at different load coefficients.

(d) The temperature field distributions of MFT at variable load condition are simulated and studied, the results show that winding temperature varies significantly with load variation, while the mutation of load coefficient does not lead to significant change of core temperature.

(e) The temperature field distributions of MFT at short circuit condition are simulated and studied, the results show that there is a sharp rise in both winding and core temperature, which is far beyond the temperature range that the transformer can withstand, which will lead to transformer damage. Therefore, the occurrence of short circuit fault should be avoided as far as possible, and protection scheme should be made to avoid transformer damage.

The temperature field analysis under various special conditions can provide the basis for the thermal design of transformer to ensure the safe operation, and the cooling schemes can be optimized according to the temperature field distribution characteristics and hot spots. Besides, the calculation of temperature field at different load coefficients can help determine the allowable load coefficient of transformer. Therefore, the research results in this paper are crucial for thermal reliability and safe operation of MFT.

Acknowledgments

This research was funded by the open project of the State Key Laboratory of Advanced Electromagnetic Engineering and Technology (China) under Grant no. 2022KF008, and the research project of Engineering Research Center for Metallurgical Automation and Measurement Technology of Ministry of Education (China) under Grant no. MADTOF2021A02.

References

[1] Guo X., et al., Inertial PLL of grid-connected converter for fast frequency support, *CSEE Journal of Power and Energy Systems*, 2022, doi: 10.17775/CSEEJPES.2021.08650

[2] Simolin, T., et al., Foundation for adaptive charging solutions: optimised use of electric vehicle charging capacity, *IET Smart Grid*, 4 (2021), 6 , pp. 599-611

[3] Guo Z. J., et al., Impact of Energy Storage on Renewable Energy Utilization: A Geometric Description, *IEEE Transactions on Sustainable Energy*, 12(2021), 2, pp. 874-885

[4] Debnath S., et al., Renewable Integration in Hybrid AC/DC Systems Using a Multi-Port Autonomous Reconfigurable Solar Power Plant (MARS), *IEEE Transactions on Power Systems*, 36(2021), 1, pp. 603-612

[5] Chen B., et al., Design Methodology for Inductor-Integrated Litz-Wired High-Power Medium-Frequency Transformer With the Nanocrystalline Core Material for Isolated DC-Link Stage of Solid-State Transformer, *IEEE Transactions on Power Electronics*, 35(2020), 11, pp. 11557-11573

[6] Beiranvand. H., et al., Vf-constrained ηρ-pareto optimisation of medium frequency transformers in ISOP-DAB converters, *IET Power Electronics*, 13(2020), 10, pp. 1984-1994

[7] Mogorovic M., and Dujic D., 100 kW, 10 kHz Medium-Frequency Transformer Design Optimization and Experimental Verification, *IEEE Transactions on Power Electronics*, 34(2019), 2, pp. 1696-1708

[8] Huang P., et al., Optimal Design and Implementation of High-Voltage High-Power Silicon Steel Core Medium-Frequency Transformer, *IEEE Transactions on Industrial Electronics*, 64(2017), 6, pp. 4391-4401

[9] Guo Z. C., et al., Design and Optimization of a 200-kW Medium-Frequency Transformer for Medium-Voltage SiC PV Inverters, *IEEE Transactions on Power Electronics*, 36(2021), 9, pp. 10548-10560

[10] Yi Z. Y., et al., Design and Optimization of the Insulation of Medium-Voltage Medium-Frequency Transformers for Solid-State Transformers, *IEEE Journal of Emerging and Selected Topics in Power Electronics*, 10(2022), 4, pp. 3561-3570

[11] Alvarez D. L., et al., Transformer Thermal Capacity Estimation and Prediction Using Dynamic Rating Monitoring, *IEEE Transactions on Power Delivery*, 34(2019), 4, pp. 1695-1705

[12] Li L. N., et al., Comprehensive Thermal Analysis of Oil-Immersed Auto-Transformer Based on Multi-Physics Analyses, *IEEE Transactions on Applied Superconductivity*, 31(2021), 8, pp. 1-5

[13] Delette G., et al., Thermal Management Design of Transformers for Dual Active Bridge Power Converters, *IEEE Transactions on Power Electronics*, 37(2022), 7, pp. 8301-8309

[14] Xu, W. L., et al., Analysis of temperature field of medium frequency transformer based on improved thermal network method, *IET Gener. Transm. Distrib*, 16(2022), 12, pp. 2346-2356

[15] Dixit A., et al., Thermal Analysis of Natural Cooling Type Distribution Transformer Retrofilled With Natural Ester Oil, *IEEE Transactions on Dielectrics and Electrical Insulation*, 29(2022), 1, pp. 231-239

[16] Shafaei R., et al., Three-Dimensional Frequency-Dependent Thermal Model for Planar Transformers in LLC Resonant Converters, *IEEE Transactions on Power Electronics*, 34(2019), 5, pp. 4641-4655

[17] Yao P. F., et al., Design Optimization of Medium-Frequency Transformer for DAB Converters With DC Bias Capacity, *IEEE Journal of Emerging and Selected Topics in Power Electronics*, 9(2021), 4, pp. 5043-5054

[18] Bahmani M. A., et al., Design Methodology and Optimization of a Medium-Frequency Transformer for High-Power DC-DC Applications, *IEEE Transactions on Industry Applications*, 52(2016), 5, pp. 4225-4233

[19] Zhang X. J., et al., Overload Distribution Transformer With Natural Ester and Aramid-Enhanced Cellulose, *IEEE Transactions on Power Delivery*, 36(2021), 3, pp. 1829-1836

[20] Wang T., et al., Three-dimensional thermal modelling of transformers in transformer room for spatial and temporal failure analysis, *IET Gener. Transm. Distrib.*, 12(2018), 13, pp. 3314-3321

[21] Xie, G. S., et al., Simulation and experimental analysis of three-dimensional temperature distribution of ±400-kV converter transformer valve-side resin impregnated paper bushing under high current, *IET Gener. Transm. Distrib.*, 16(2022), 15, pp. 2989-3003

[22] Chen H. and Xu Y., Electromagnetic field analysis coupled model of fluid–structure–thermal simulation of power converter for switched reluctance machine, *IEEE Transactions on Applied Superconductivity*, 26(2016), 4, pp. 1-6

[23] Li, X. L., et al., Temperature and electric field distribution of tri-post insulator in DC-GIL based on numerical multiphysics modelling, *IET Gener. Transm. Distrib.* 17(2022), 6, pp. 1232-1242

Submitted: 7.8.2023.

Revised: 5.9.2023.

Accepted: 21.9.2023